Electronic Supplementary Material (ESI) for Journal of Materials Chemistry A.

Supporting information

Fluffy carbon-coated red phosphorus as a highly stable and high rate anode for lithium ion batteries

Huan Liu [a,1], Shixue Zhang [b,1], Qizhen Zhu [b], Bin Cao [b], Renjie Chen [a,*], Peng Zhang [b], Ning Sun [b], Bin Xu [b,*], Feng Wu [a]

[a] School of Materials Science & Engineering, Beijing Key Laboratory of Environmental Science and Engineering, Beijing Institute of Technology, Beijing 100081, China. *E-mail: chenrj@bit.edu.cn (R. Chen)

[b] State Key Laboratory of Organic-Inorganic Composites, Beijing Key Laboratory of Electrochemical Process and Technology for Materials, Beijing University of Chemical Technology, Beijing 100029, China. *E-mail: xubin@mail.buct.edu.cn, binxumail@163.com (B. Xu).

H. Liu and S. Zhang contributed equally to this paper.

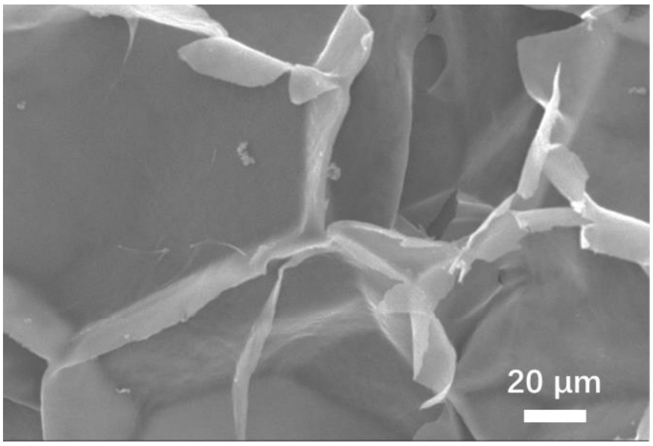

Fig. S1 SEM images of the FC.

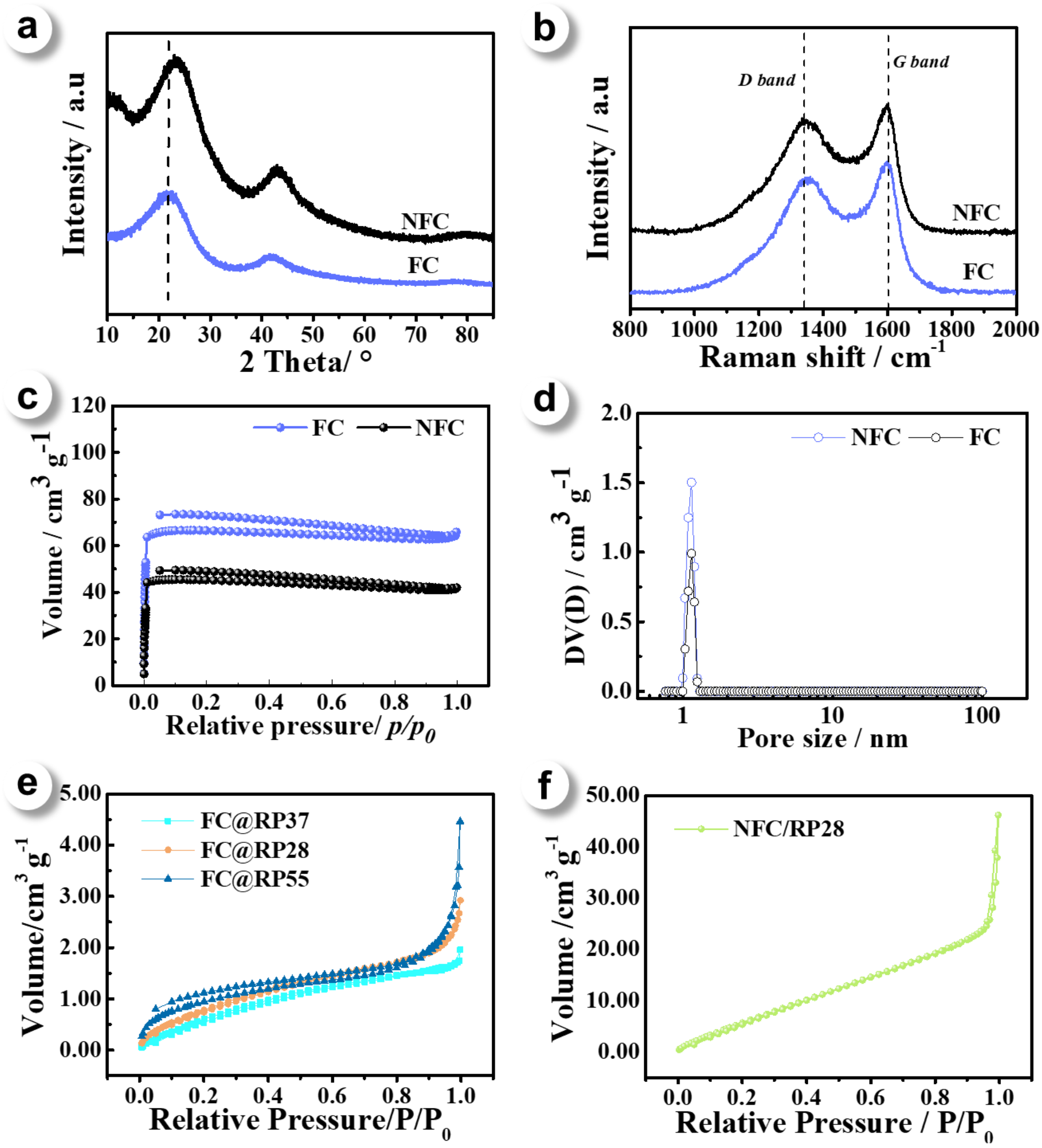

Fig. S2 XRD (a), Raman (b) spectra, nitrogen adsorption-desorption isotherms (c, e, f) and the pore size distribution (d) for FC and NFC sample.

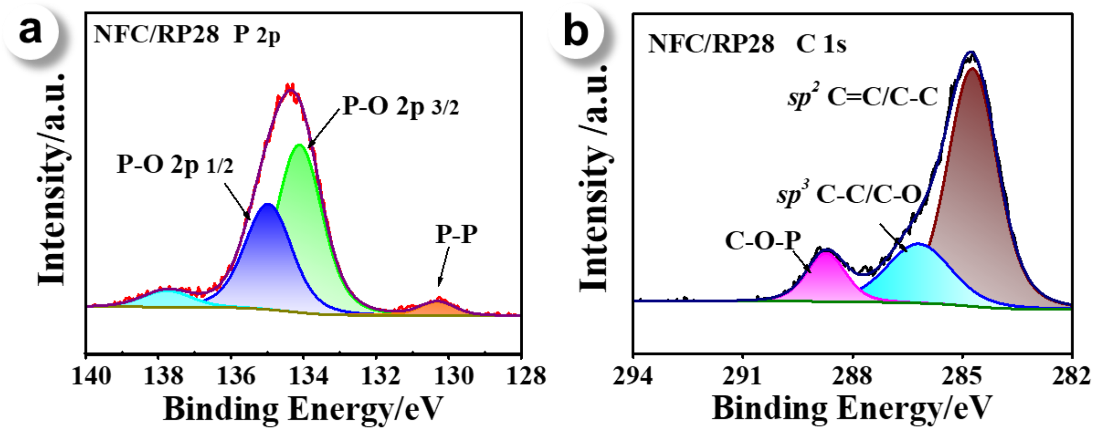

Fig. S3 XPS of P 2p (a) and C 1s (b) for NFC/RP28.

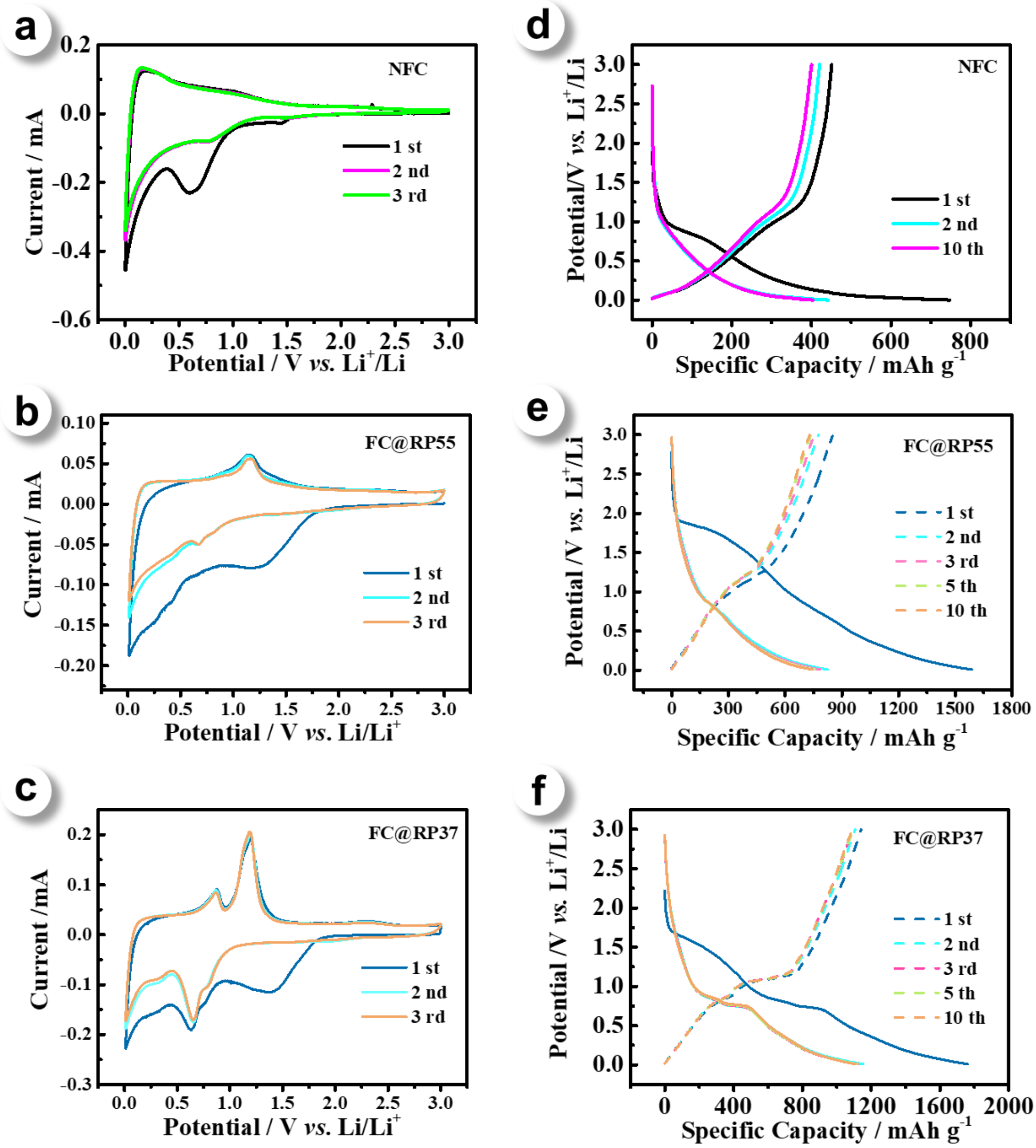

Fig. S4 The CV curves of NFC (a), FC@RP55 (b) and FC@RP37 (c) at a scan rate of 0.1 mV s^{-1}. Voltage profiles of NFC (d) at the current density of 0.1C (1C=372 mAh g^{-1}), FC@RP55 (e), and FC@RP37 (f) at 0.05C (1C=2600 mA g^{-1}).

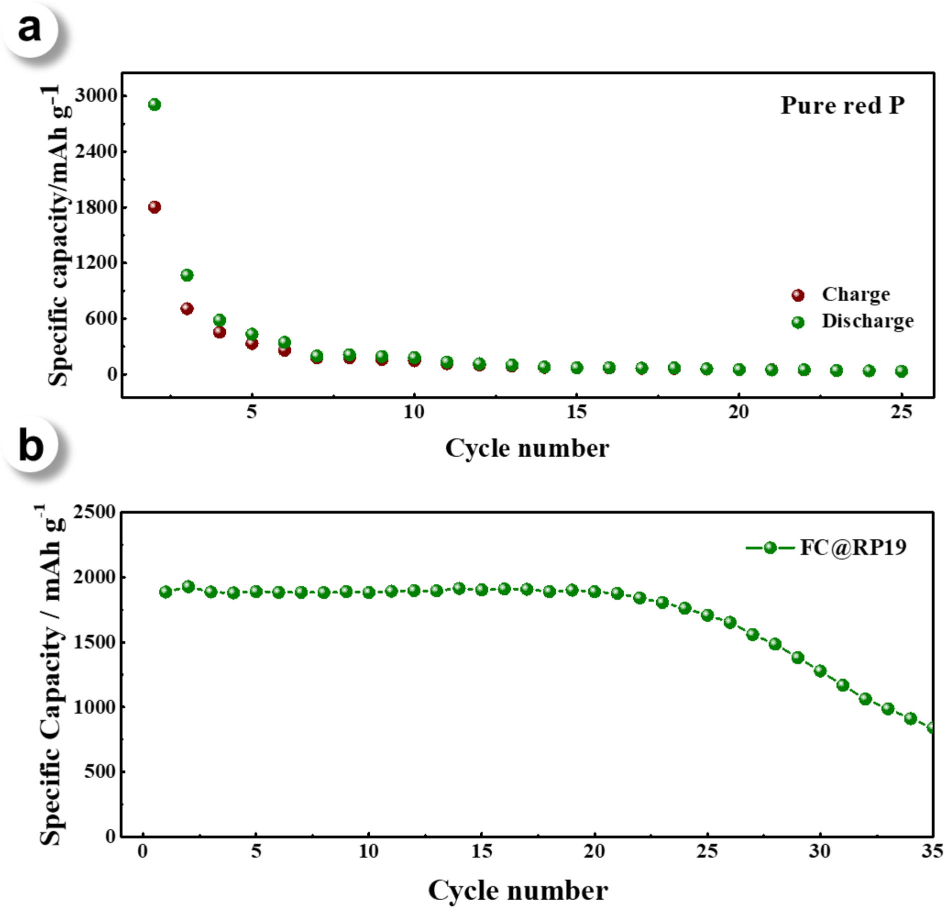

Fig. S5 Cycle performance of pure red P and FC@RP19 electrode at 0.05C.

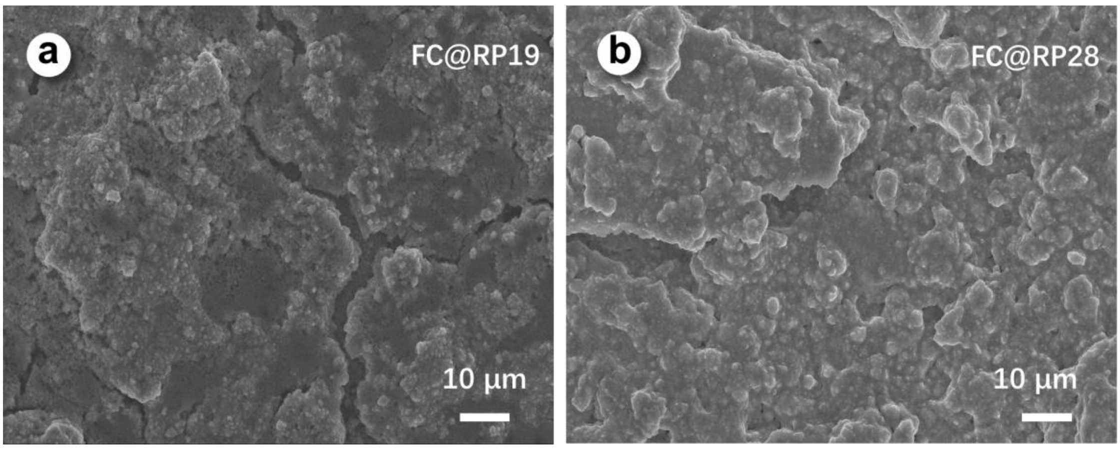

Fig. S6 SEM images of FC@RP19 and FC@RP28 electrodes after 20th cycle.

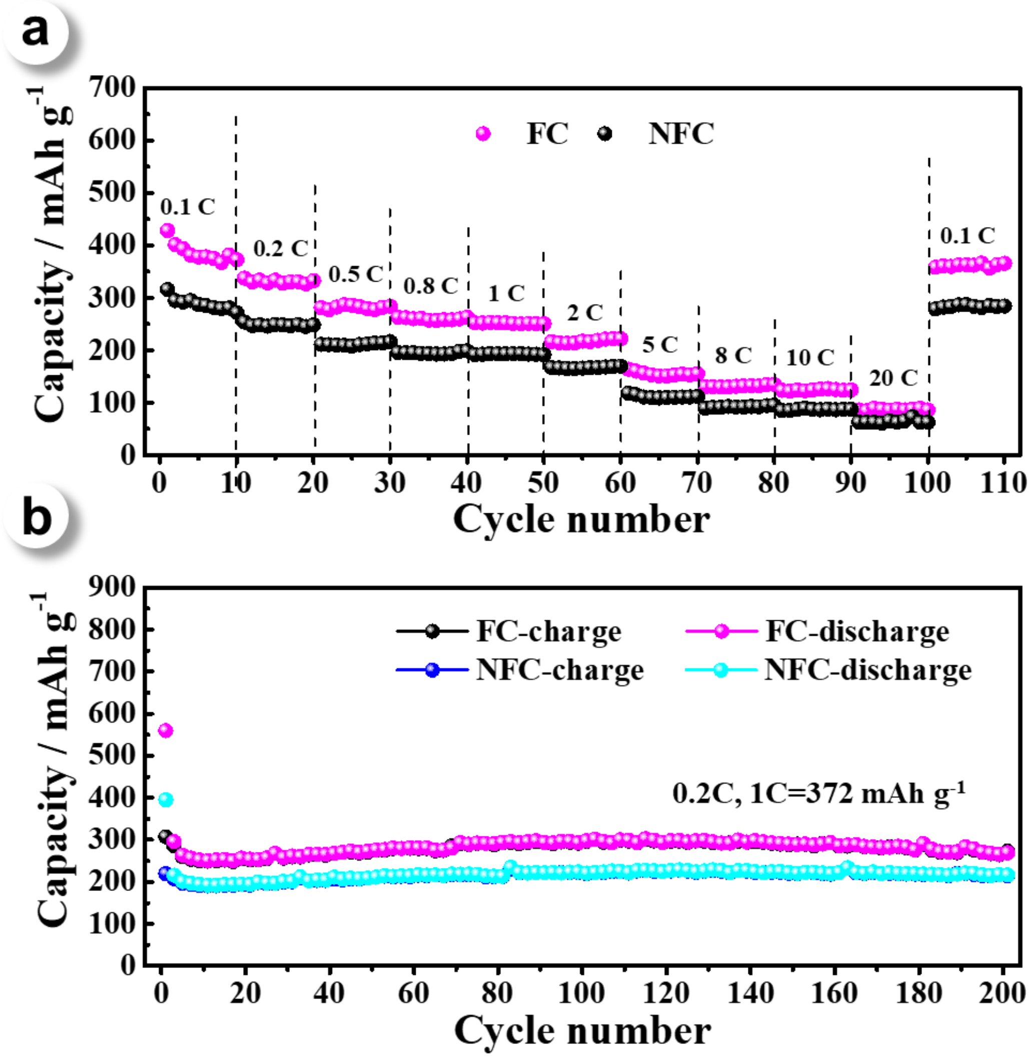

Fig. S7 Rate performance of FC and NFC at different current density (a). Cycle performance of FC and NFC electrode at a current density of 1C (372 mA g^{-1}).

Table S1. Electrochemical performance comparison of phosphorus/carbon composites as anode for lithium-ion batteries.

Sample	P/C ratio *or* P wt %	Preparation method	Initial charge capacity / mAh g^{-1}	Cycle performance	Ref.
Ring-shaped phosphorus/ MWCNTs	16	Vapor phase reaction	1206 at 0.5 A g^{-1}	58.8 % capacity retention over 10 cycle	[1]
Red phosphorus/graphene	40	Electro-spraying and far-infrared reduction	~1763 at 0.1 A g^{-1}	Capacity of ~1542 mAh g^{-1} is retained after 100 cycles	[2]
Red P/ carbon film	21	Vapor phase polymerization	~1511 at 0.1 A g^{-1}	Capacity of 903 mAh g^{-1} after 640 cycles	[3]
Hollow red-phosphorus nanospheres	60	Wet solvothermal method	1285.7 at 0.52 A g^{-1}	Capacity (based on P) of 1048.4 mA h g^{-1} at 1 C after 600 cycles	[4]
Red phosphorus/RGO films	10	Sonication technique	~850 at 50 mA g^{-1}	Capacity of 706 mA h g^{-1} at 50 mA g^{-1} after 200 cycles.	[5]
Phosphorus/ carbon nanotubes	70	Wet ball-milling	1396.6 at 50 mA g^{-1}	~90 % capacity retention over 50 cycles.	[6]
Phosphorus/carbon composites	60	Ball-milling	1585.3 mAh g^{-1} at 0.1 C	Capacity retention of 68.3% over 200 cycles	[7]
Phosphorus/graphene composites	80	Solution-based method	~1555 mAh g^{-1} at 0.2 A g^{-1}	Capacity of 1286 mA h g^{-1} after 100 cycles at 0.2 A g^{-1}	[8]
Phosphorus/active carbon	47	Vaporization–condensation	2130 mAh g^{-1} at 0.15A g^{-1}	Capacity of 1370 mAh g^{-1} after 85 cycles at 0.3 A g^{-1}	[9]
Phosphorus/ carbon nanotubes	80	Ball-milling	2133.4 mA h g^{-1} at 0.05C	Capacity of 998.5 mAh g^{-1} after 50 cycles	[10]
Phosphorus/graphene	70	High-pressure-assisted spraying	1876 mAh g^{-1} at 50 mA g^{-1}	Capacity of 990 mAh g^{-1} after 50 cycles	[11]
Amorphous red phosphorus@ fluffy hard carbon composites	80	Ball-milling	1699.5 mAh g^{-1} at 0.05C	~1230 mAh g^{-1} at 1C over 1000 cycles with 96% of capacity retention	This work

Table S2. The R_s and R_{ct} for all the FC@RP electrodes.

Sample	R_S/Ohm	R_{ct}/Ohm
FC@RP19	4.18	135.9
FC@RP28	4.09	43.13
FC@RP37	4.02	48.67
FC@RP55	3.92	77.58

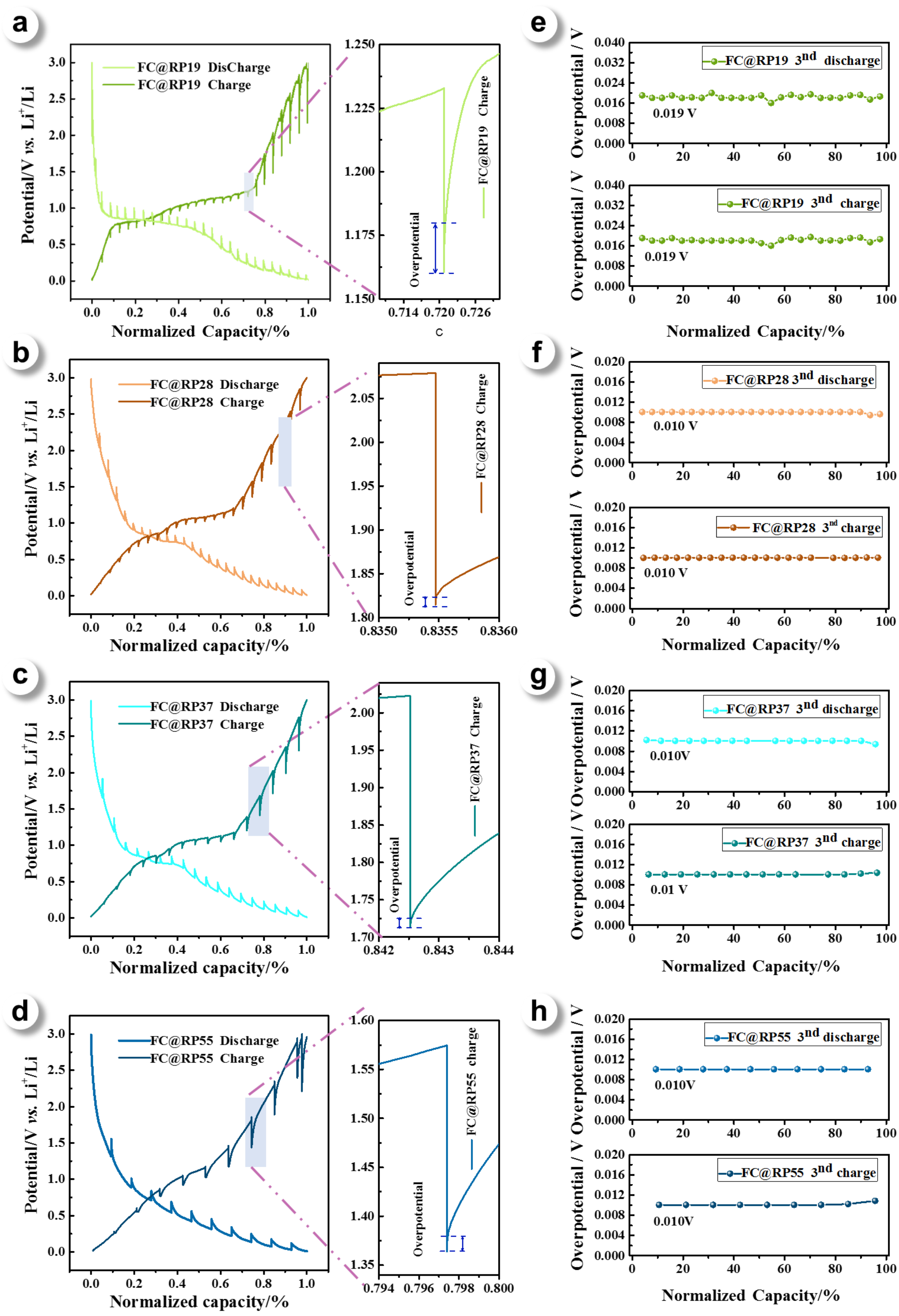

Fig. S8 The potential response curves of FC@RP during GITT measurements with the inset of the magnified area illustrating the overpotential (a-d). Overpotential values estimated from the GITT results for 5th cycle (e-h).

The cell voltage is linearly proportional to $\sqrt{\tau}$, as shown in Figure S8b. The diffusion coefficient (D) can be calculated from the GITT potential profiles by Fick's second law, as the following equation:

$$D = \frac{4}{\pi\tau}\left(\frac{m_B V_M}{M_B S}\right)^2\left(\frac{\Delta E_S}{\Delta E_\tau}\right)^2 \qquad \text{(equation S1)}$$

The τ is the titration time, m_B is the electrode active material mass, S is the geometric area of the Cu foil electrode, ΔE_S is the quasi-thermodynamic equilibrium potential difference before and after the current pulse, ΔE_τ is the potential difference during current pulse, V_M is the molar volume, M_B is the molar mass.

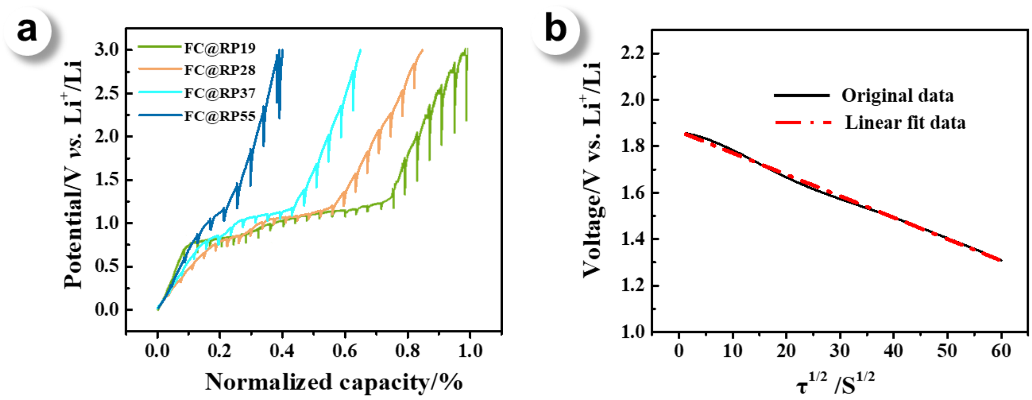

Fig. S9 GITT profile of the FC@ RP electrodes in the charge state (a), and linear behavior of the potential *vs.* $\sqrt{\tau}$ relationship in GITT at 1.824 V *vs.* Li^+/Li of forth lithiation process of FC@RP28 for LIBs.

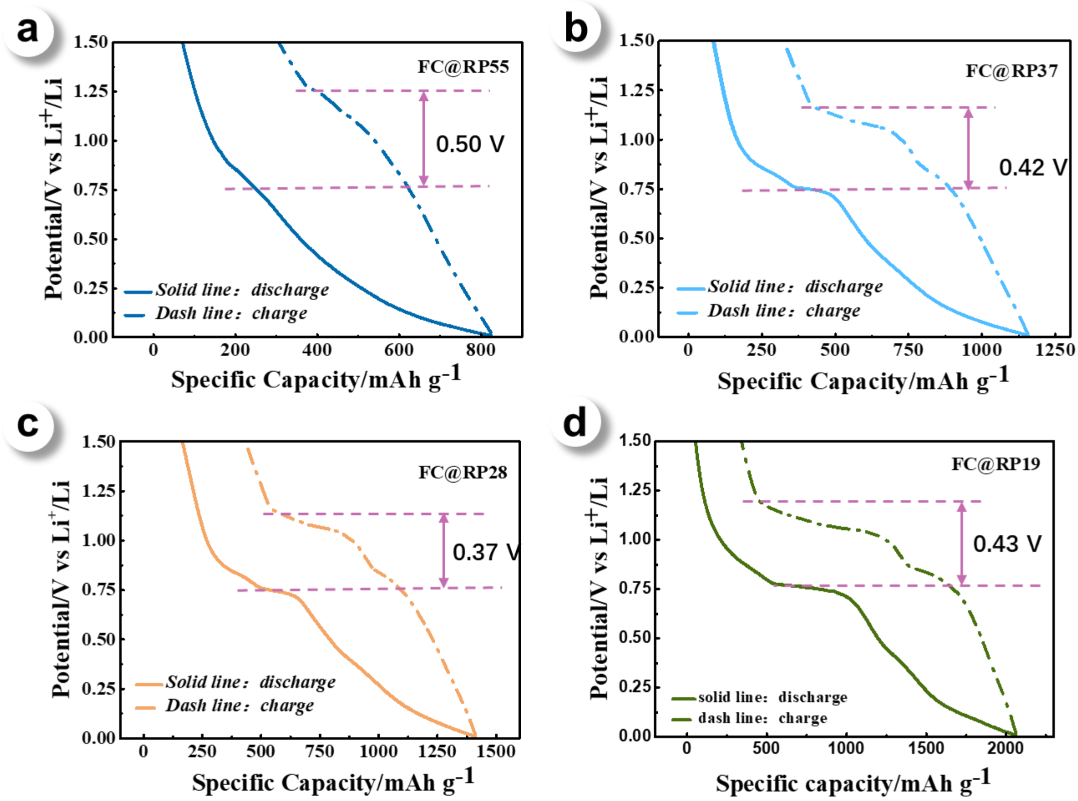

Fig. S10 Voltage profiles of all FC@RP electrodes show the voltage hysteresis between the charge and discharge at 1C.

Reference

[1] D. Zhao, J. Zhang, C. Fu, J. Huang, D. Xiao, M.M.F. Yuen, C. Niu, Enhanced cycling stability of ring-shaped phosphorus inside multi-walled carbon nanotubes as anodes for lithium-ion batteries, Journal of Materials Chemistry A 6(6) (2018) 2540-2548.

[2] Z. Yue, T. Gupta, F. Wang, C. Li, R. Kumar, Z. Yang, N. Koratkar, Utilizing a graphene matrix to overcome the intrinsic limitations of red phosphorus as an anode material in lithium-ion batteries, Carbon 127 (2018) 588-595.

[3] J. Ruan, T. Yuan, Y. Pang, X. Xu, J. Yang, W. Hu, C. Zhong, Z.F. Ma, X. Bi, S. Zheng, Red Phosphorus-Embedded Cross-Link-Structural Carbon Films as Flexible Anodes for Highly Reversible Li-Ion Storage, ACS applied materials & interfaces 9(41) (2017) 36261-36268.

[4] J. Zhou, X. Liu, W. Cai, Y. Zhu, J. Liang, K. Zhang, Y. Lan, Z. Jiang, G. Wang, Y. Qian, Wet-Chemical Synthesis of Hollow Red-Phosphorus Nanospheres with Porous Shells as Anodes for High-Performance Lithium-Ion and Sodium-Ion Batteries, Advanced materials 29(29) (2017).

[5] C.M. Subramaniyam, Z. Tai, N. Mahmood, D. Zhang, H.K. Liu, J.B. Goodenough, S.X. Dou, Unlocking the potential of amorphous red phosphorus films as a long-term stable negative electrode for lithium batteries, J. Mater. Chem. A 5(5) (2017) 1925-1929.

[6] Z. Xu, Y. Zeng, L. Wang, N. Li, C. Chen, C. Li, J. Li, H. Lv, L. Kuang, X. Tian, Nanoconfined phosphorus film coating on interconnected carbon nanotubes as ultrastable anodes for lithium ion batteries, Journal of Power Sources 356 (2017) 18-26.

[7] J. Xu, I.-Y. Jeon, J. Ma, Y. Dou, S.-J. Kim, J.-M. Seo, H. Liu, S. Dou, J.-B. Baek, L. Dai, Understanding of the capacity contribution of carbon in phosphorus-carbon composites for high-performance anodes in lithium ion batteries, Nano Research 10(4) (2017) 1268-1281.

[8] L. Sun, Y. Zhang, D. Zhang, Y. Zhang, Amorphous red phosphorus nanosheets anchored on graphene layers as high performance anodes for lithium ion batteries, Nanoscale 9(46) (2017) 18552-18560.
[9] J. Li, L. Wang, X. He, J. Wang, Effect of Pore Size Distribution of Carbon Matrix on the Performance of Phosphorus@Carbon Material as Anode for Lithium-Ion Batteries, ACS Sustainable Chemistry & Engineering 4(8) (2016) 4217-4223.
[10] D. Yuan, J. Cheng, G. Qu, X. Li, W. Ni, B. Wang, H. Liu, Amorphous red phosphorous embedded in carbon nanotubes scaffold as promising anode materials for lithium-ion batteries, Journal of Power Sources 301 (2016) 131-137.
[11] L. Wang, H. Guo, W. Wang, K. Teng, Z. Xu, C. Chen, C. Li, C. Yang, C. Hu, Preparation of sandwich-like phosphorus/reduced graphene oxide composites as anode materials for lithium-ion batteries, Electrochimica Acta 211 (2016) 499-506.